Reexamining equations of state of oblate hard ellipsoids of revolution: Numerical simulation utilizing a cluster Monte Carlo algorithm and comparison to virial theory

Philipp Marienhagen and Joachim Wagner*
Institut für Chemie, Universität Rostock, 18059 Rostock, Germany

(Received 29 November 2021; accepted 5 January 2022; published 25 January 2022)

We provide highly accurate equation-of-state data determined by means of cluster Monte Carlo simulations for the isotropic phase of oblate hard ellipsoids of revolution. Both equation-of-state data and phase boundaries of the isotropic phase are obtained from relatively large ensembles with typically 1000 particles. The comparison of simulation data with a virial approach gives evidence for the importance of high-order so-far-unknown virial coefficients and therewith many-particle interactions in dense, isotropic systems of anisotropic particles. While a virial approach with a rescaled Carnahan-Starling correction for the unknown, higher-order virial coefficients reproduces the simulation data of moderately anisotropic particles with high accuracy, we suggest for highly anisotropic shapes a simple, heuristic equation of state as a suitable approach.

DOI: 10.1103/PhysRevE.105.014125

I. INTRODUCTION

Due to their relevance as model systems for dense condensed matter, hard-particle systems have attracted large scientific interest for several decades. In addition to hard-sphere systems, where numerous properties can be calculated analytically, with increasing computer performance a growing interest in anisometric hard-particle systems emerged. Using computer simulations considering realistic many-particle interactions, Onsagers theory on isotropic-nematic phase transitions [1] could be confirmed and extended. To obtain an analytical access to this phase transition, Onsager used infinitely thin needles as a model. With computer simulations, which are capable to handle different particle shapes, the investigation of the influence of the detailed particle geometry and its aspect ratio ν is possible. Herewith, tunable models for the self-organization and properties of liquid crystalline matter could be investigated.

First computer simulations of hard ellipsoids [2,3] identified an isotropic-nematic phase transition depending on the aspect ratio and provided first equation-of-state data for these systems. The identification of unusual dense packings of ellipsoids exceeding even close packings of spheres [4] initiated a reexamination of the hard ellipsoid system concerning both equation of state [5] and phase behavior for the identified structures. In addition to an isotropic and nematic phase, a plastic crystalline phase and the unusually dense monoclinic SM2 phase could be identified as two types of crystalline phases [6–9].

The theoretical investigation of hard-sphere systems simultaneously stimulated the development and refinement of simulation techniques. Starting from the seminal Metropolis-Hastings scheme [10,11] as a theoretical background of classical Monte Carlo (MC) simulations, improved methods such as biased MC simulations [12], event-chain Monte Carlo [13–15], and replica exchange Monte Carlo methods [16] have been developed.

Especially for the simulation of hard-body multiparticle systems in the isobaric and isothermal (N, p, T) ensemble, cluster MC as a variant of biased MC simulations is the method of choice to calculate accurate equation-of-state data as shown by Almarza [17] for the crystalline phase of hard-sphere systems. This method has been extended to anisotropic particles to investigate the phase behavior of hard rhombic platelets [18]. The availability of theoretical predictions for the phase behavior and equation of state has regularly lead to experimental verifications employing colloidal model systems with predominant hard-body interactions by means of scattering methods [19] or confocal microscopy [20].

The virial series is a complementary theoretical approach to equation-of-state data of the isotropic phase of hard multiparticle systems. While the second virial coefficients of convex hard bodies are analytically known [21–24], higher virial coefficients have to be calculated employing numerical methods [25,26]. With an optimized algorithm based on Mayer sampling [27], these quantities are accessible with improved accuracy [28]. In contrast to MC simulations of large ensembles, for the calculation of the virial coefficient of order i, a cluster integral over interactions between i particles is calculated. Since the maximum order of accessible virial coefficients is limited, the truncation of the virial series at order $i_{\max}$ ignores contributions of clusters with $N > i_{\max}$ particles to the equation of state.

The Carnahan-Starling relation $B_i^* = i^2 + i - 2$ as an approximation for the reduced virial coefficients of order i leads to a closed expression for hard spheres' equation of state in terms of their volume fraction $\varphi = \varrho V_P$, where ϱ denotes the number density of particles and V_P the particle volume. Parsons suggested rescaling the hard-sphere virial coefficients by the ratio of the reduced, second virial coefficient of an anisotropic shape and a sphere as an approximation for the

*joachim.wagner@uni-rostock.de

equation of state of an ensemble of anisotropic particles [29]. Later, Vega [25] modified this approach considering all known virial coefficients and approximating only the unknown ones in the same manner. Alternatively, several heuristic correlations for the equation of state have been suggested [30–33].

Since cluster-MC simulations give access to precise equation-of-state data and implicitly take many-particle interactions of large systems into account, with these data, a systematic evaluation of proposed equations of state and corrections for the truncated virial series is possible.

II. THEORETICAL BACKGROUND

A. (N, p, T) Monte Carlo algorithm

Monte Carlo simulations in the isobaric-isothermal (N, p, T) ensemble are a useful approach to determine equation-of-state data of hard particles as already proposed by McDonald [34]. In this ensemble with fixed pressure p, Monte Carlo simulations compute the configuration integral of the studied system which is independent of the thermal energy $\beta^{-1} = k_B T$ since the potential energy $U(\mathbf{r}^N, V)$ can in the case of hard particles only be infinite in an overlapping configuration or zero otherwise. In the following, for better readability, only the potential energy's dependence on the center-of-mass coordinates $\mathbf{r}^N$ is explicitly written down, which can easily be extended to anisotropic systems by additionally introducing angular coordinates.

To simulate an (N, p, T) ensemble, fluctuations of the system's volume V and therewith the simulation box are necessary. Employing a transformation matrix $\mathbf{H}$ defined by $\mathbf{r}_i = \mathbf{H}.\mathbf{s}_i$, volume-independent, reduced center-of-mass coordinates $\mathbf{s}_i$ are elegantly obtained allowing particle moves decoupled from volume changes of the simulation box. The volume of the simulation box equals the parallelepipedal product $V = \|\mathbf{H}\|$ of the transformation matrix.

In the case of fluid phases, where a cubic simulation box can be used, the transformation matrix is simply related to matrix identity $\mathbf{I}$ via $\mathbf{H} = V^{\frac{1}{3}}\mathbf{I}$. For the simulation of solid phases, additionally shape fluctuations of the simulation box are required for which an upper triangular transformation matrix $\mathbf{H}$ is an obvious choice enabling decoupled shape and volume fluctuations.

B. Acceptance criteria for volume fluctuations

Starting from the configuration integral

$$Z_{N,p,T} = \int_V V^{N-1} \int_{\mathbf{s}_1} \cdots \int_{\mathbf{s}_N} \times \exp[-\beta pV - \beta U(\mathbf{s}^N, V)] d^N\mathbf{s}\, dV, \quad (1)$$

the normalized probability of a configuration $(\mathbf{s}^N, V)$ reads as

$$p_{N,p,T}(\mathbf{s}^N, V) = \frac{V^{N-1}}{Z_{N,p,T}} \exp[-\beta pV - \beta U(\mathbf{s}^N, V)] \quad (2)$$

with the reduced enthalpy as argument of the exponential. Herewith, the acceptance criterion $P_A(V'|V)$ for a volume change from V to V' in an (N, p, T) ensemble can be written as

$$P_A(V'|V) = \min\left[1, \left(\frac{V'}{V}\right)^{N-1} \frac{\exp[-\beta pV' - \beta U(\mathbf{s}^N, V')]}{\exp[-\beta pV - \beta U(\mathbf{s}^N, V)]}\right] \quad (3)$$

within the Metropolis-Hastings scheme [35].

C. Cluster MC algorithm

To improve the sampling efficiency, Almarza adopted a cluster algorithm for the (N, p, T) simulation of hard spheres [17]. In this approach, the biased formation of rigid pseudomolecules of especially close particles during volume fluctuations increases the accepted mean volume change $\langle|V' - V|\rangle$ and thus allows a better exploration of phase space. Before the actual volume change random bonds are generated between particles forming clusters containing all pairs of all linked particles. Instead of scaling the particles coordinates during a volume trial move, only the cluster's center of mass is rescaled, preserving the interparticle distances and orientations within the rigid cluster.

The arbitrary bond probability function $b(r_{ij})$ suggested by Almarza was generalized by Tasios [18] to anisotropic particles

$$b(\sigma_{ij}) = \begin{cases} 1 - \left(\frac{\sigma_{ij}}{\delta}\right)^2 & : \quad \sigma_{ij} < \delta \\ 0 & : \quad \sigma_{ij} \geqslant \delta \end{cases} \quad (4)$$

by considering the shortest surface distance σ_{ij} instead of the center-of-mass distance r_{ij}. Using the closest surface distance σ_{ij} weighted by the cutoff distance δ increases the probability of forming clusters at small surface distances while for distances $\sigma_{ij} \geqslant \delta$ bonds are not generated.

Since the probability of forming a specific cluster configuration depends via the surface distances σ_{ij} on the volume, an additional factor in the acceptance probability is required to fulfill the condition of detailed balance. Let $\omega_c(\chi_c|\mathbf{s}'^N, V')$ be the probability to form the cluster configuration χ_c at reduced center-of-mass configuration $\mathbf{s}'^N$ and volume V', and $\omega_c(\chi_c|\mathbf{s}^N, V)$ that with reduced center-of-mass configuration $\mathbf{s}^N$ at volume V, the acceptance probability for a volume change allowing cluster formation reads as

$$P_A(V'|V, \chi_c) = \min\left[1, \left(\frac{V'}{V}\right)^{\tilde{N}-1} \frac{\exp[-\beta pV' - \beta U(\chi_c, V')]}{\exp[-\beta pV - \beta U(\chi_c, V)]} \times \frac{\omega_c(\chi_c|\mathbf{s}'^N, V')}{\omega_c(\chi_c|\mathbf{s}^N, V)}\right] \quad (5)$$

under the constraint of detailed balance. Additionally, the apparent number of particles $\tilde{N} \leqslant N$ is reduced by cluster formation, where $\tilde{N}$ is the sum of remaining single particles and the number of present clusters.

The additional factor in the volume change proposal ratio allowing cluster formation can, according to Almarza [17], be written as

$$\frac{\omega_c(\chi_c|\mathbf{s}'^N, V')}{\omega_c(\chi_c|\mathbf{s}^N, V)} = \prod_{[ij]} \frac{1 - b(\sigma'_{ij})}{1 - b(\sigma_{ij})}, \quad (6)$$

where the product contains factors resulting from all particle combinations $[ij]$ where i and j belong to different clusters.

However, there is no need to check that i and j belong to different clusters: Since, within a cluster, interparticle distances and relative orientations are preserved during a volume change, the surface distances $\sigma'_{ij} = \sigma_{ij}$ remain unchanged, resulting in $[1 - b(\sigma'_{ij})]/[1 - b(\sigma_{ij})] = 1$. For large systems, the numerical stability can be improved by calculating the product by the summation of individual ratios' logarithms.

Using periodic boundary conditions, particles within a cluster may be linked via a chain of bonds to its periodic images. When this cluster percolation occurs, the simulation box cannot be rescaled, keeping the particle distances within the cluster constant. Hence cluster percolation has to be checked and volume change attempts leading to cluster percolation have to be rejected. If the amount of scale rejections becomes substantial, the sampling efficiency of cluster-MC simulations decreases.

D. Surface distance of ellipsoids

The check for overlaps of two ellipsoids can be done by the Perram-Wertheim algorithm [36]. This algorithm essentially scales two ellipsoids until they reach tangent contact. From the scaling factor at tangent contact, overlap and nonoverlap can be distinguished. We improved the performance of the original algorithm by replacing the bisection minimization by a Newton-Raphson minimization using analytic derivatives of the elliptic contact function.

There is no known algorithm to directly determine the closest surface distance $\sigma(\mathbf{A}, \mathbf{B})$ of two ellipsoids $\mathbf{A}$ and $\mathbf{B}$ with given shape, orientation, and center of mass which is needed to calculate the bond probability. Paramonov and Yaliraki [37] suggested a lower limit $\sigma_{\mathrm{ll}}(\mathbf{A}, \mathbf{B})$ and an upper limit $\sigma_{\mathrm{ul}}(\mathbf{A}, \mathbf{B})$ for the closest surface distance $\sigma(\mathbf{A}, \mathbf{B})$ fulfilling the inequality

$$0 < \sigma_{\mathrm{ll}}(\mathbf{A}, \mathbf{B}) \leqslant \sigma(\mathbf{A}, \mathbf{B}) \leqslant \sigma_{\mathrm{ul}}(\mathbf{A}, \mathbf{B}) \tag{7}$$

for nonoverlapping particles. The upper limit $\sigma_{\mathrm{ul}}(\mathbf{A}, \mathbf{B})$ can be directly determined in the Perram-Wertheim algorithm and is a reasonable approximation for large distances. In the limit $\sigma_{\mathrm{ul}}(\mathbf{A}, \mathbf{B}) \to \infty$, the approximation is independent of the mutual orientation of both ellipsoids. The lower limit $\sigma_{\mathrm{ll}}(\mathbf{A}, \mathbf{B})$ can be determined by calculating the projection of the upper limit to the normal vector of both rescaled ellipsoids at the common contact point. The latter approximation generally provides better results for small separations.

Therefore, the lower limit $\sigma_{\mathrm{ll}}(\mathbf{A}, \mathbf{B})$ is expected to be a better approximation in the case of small surface distances, when clusters are presumably formed. However, obvious differences between the results of cluster-MC simulations using both approximations for σ_{ij} are not observed within their uncertainties. We presume that the proposal ratio in Eq. (6) sufficiently compensates over- and underestimations of the surface distance. The data provided in this contribution are obtained using the lower limit $\sigma_{\mathrm{ll}}(\mathbf{A}, \mathbf{B})$ as an approximation for the closest surface distance.

E. Simulation details

An isotropic start configuration is prepared for each investigated pressure via an equilibration phase of 10^6 MC steps at a volume fraction of $\varphi = 0.05$ starting from a configuration with centers of mass placed at a cubic lattice and particle directors randomly aligned, where an MC step consists of N particle translation or rotation attempts and a volume change attempt.

The resulting isotropic configuration is compressed to the pressure of interest and after a second equilibration phase a production run with 5×10^7 steps is performed.

Since cluster percolation is an increasing obstacle for the simulation of highly anisotropic particles, the characteristic length δ which determines cluster formation is tuned to obtain approximately $N_{\mathrm{b}}/N \approx 1/4$, where N_{b} is the number of bonds created between N individual particles. Hereby the number of rejections due to cluster percolation is reduced to less than 1%.

Since isotropic-crystalline phase transitions can only be determined by the expansion of a crystalline phase, these phase boundaries are determined by expansion of a dense monoclinic SM2 crystal [38] containing between 972 and 1040 particles depending on their aspect ratio. For these expansion simulations, additionally shape fluctuations of the simulation box at constant volume are allowed, where at least 2×10^8 steps are performed.

III. RESULTS AND DISCUSSION

A. Validation of the cluster-MC algorithm with a system of hard spheres

As hard spheres are a thoroughly investigated model system, the cluster (N, p, T) algorithm is validated with hard spheres, i.e., ellipsoids with an aspect ratio $\nu = 1$. The deviations of our data from the highly accurate equation-of-state data of Kolafa *et al.* [39] are illustrated in Fig. 1 for five different system sizes from $N = 500$ to $N = 2916$.

A comparison of the different system sizes shows that the system-size dependence becomes more pronounced with increasing reduced pressure $\beta\, pr^3$. This is especially the case in the region of the phase transition, which is indicated by the dashed black line (as determined by Noya *et al.* [40]). The data beyond the phase transition result from a metastable phase and depend significantly on the system size. While this dependence is especially notable for $N = 500$ particles, it decreases for $N = 864$ particles and the deviations are within the determined uncertainties of the volume fraction φ compared to the equation of state of Kolafa *et al.* for larger systems. It is also visible that the determined uncertainties for a system of $N = 864$ hard spheres obtained in 5×10^7 steps employing the cluster algorithm displayed with blue error bars are considerably smaller than those obtained in 2.5×10^8 steps displayed with gray error bars employing a standard (N, p, T) approach. Although equation-of-state data for hard spheres can be determined via simpler methods, the comparison with the data shown in Fig. 1 is a proof of the cluster algorithm's reliability.

For anisotropic particles only few data are available resulting from relatively small ensembles. A comparison of available data from McBride and Lomba [5] with our cluster-MC data is displayed in the Supplemental Material (Sec. S-I) [41].

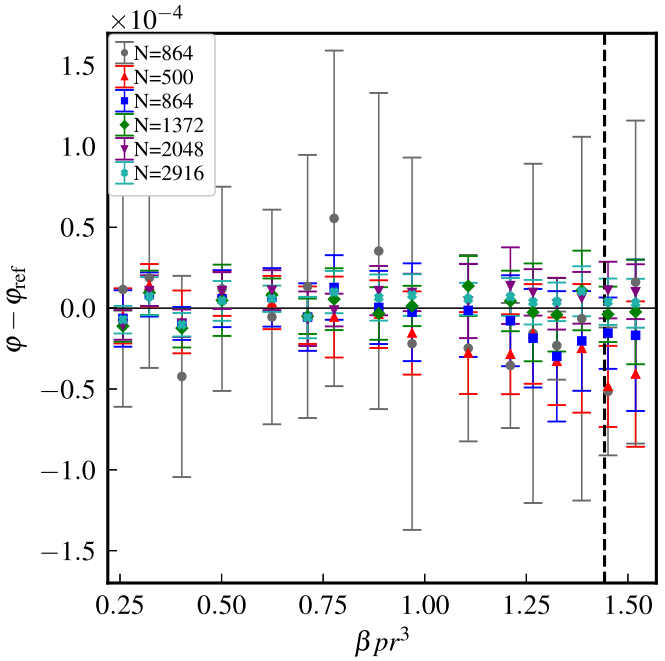

FIG. 1. Deviations of hard-sphere volume fraction φ from the reference data φ_{ref} from Kolafa *et al.* [39] in dependence on the reduced pressure βpr^3. The volume fractions are determined for five system sizes N obtained during 5×10^7 steps with the cluster (N, p, T) algorithm. For comparison, data obtained during 2.5×10^8 steps in a classical (N, p, T) MC simulation are displayed with dark gray circles. The liquid-solid phase transition of hard spheres determined by Noya *et al.* [40] is indicated by the dashed black line.

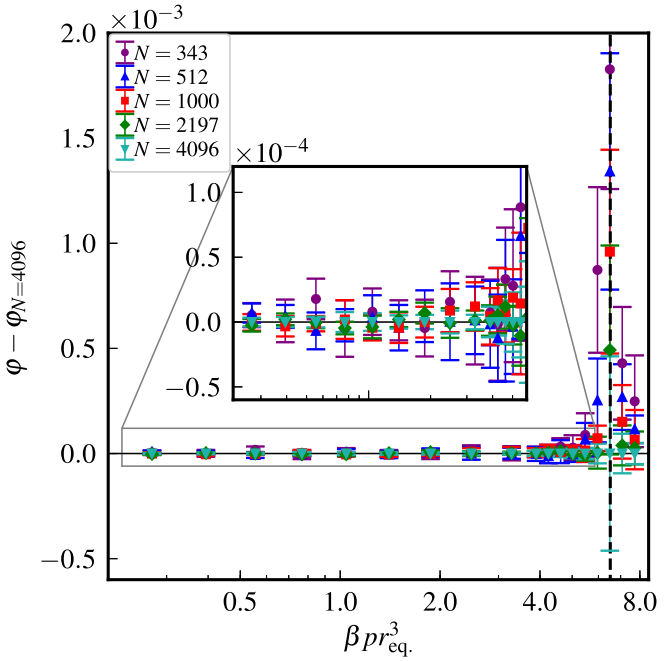

FIG. 2. Deviations of the volume fraction φ in dependence on the reduced pressure βpr^3_{eq} for aspect ratio $\nu = 1/3$ using different system sizes N. Here, the largest investigated system with $N = 4096$ particles is used as a reference. The estimated critical pressure for the isotropic-nematic phase transition is indicated by the dashed black line.

B. Influence of the system size for aspect ratio $\nu = 1/3$

The influence of the system size is exemplarily investigated for the intermediate aspect ratio $\nu = 1/3$. Data from five different system sizes from $N = 343$ to $N = 4096$ are analyzed in Fig. 2, where deviations of volume fractions are displayed in dependence on the reduced pressure. As a reference, data of the largest investigated system with $N = 4096$ particles are used.

For reduced pressures βpr^3_{eq} below the isotropic-nematic phase transition, a systematic dependence of the volume fraction φ on the system size cannot be observed. In the phase transition's vicinity, however, a significant system-size dependence emerges. Additionally, the uncertainties increase drastically in this region.

For the subsequent systematic investigation of equations of states in dependence on the aspect ratio ν, systems with $N = 1000$ particles are used. The deviations to a system of $N = 4096$ particles are in the range of the uncertainties at acceptable numerical effort. Equation-of-state data obtained for these systems with aspect ratios $1/10 \leqslant \nu \leqslant 1$ are compiled in Tables S-1, S-2, S-3, and S-4 in the Supplemental Material (Sec. S-II) [41].

C. Tracing the phase transitions

Since phase transitions are discontinuities in equations of state, the regions of stability need to be determined as a first step. For the equation of state in the isotropic phase of oblate ellipsoids of revolution, phase boundaries to nematic, plastic solid, and monoclinic phase limit their region of stability depending on the aspect ratio. The formation of these phases can be identified by means of characteristic observables.

1. Isotropic-nematic phase transition

The formation of nematic phases is identified by the nematic order parameters S_2 and S_4 defined as averages

$$S_2 = \left\langle \frac{1}{2}\left(3x_i^2 - 1\right)\right\rangle_{x_i}, \tag{8}$$

$$S_4 = \left\langle \frac{1}{8}\left(35x_i^4 - 30x_i^2 + 3\right)\right\rangle_{x_i}, \tag{9}$$

of the second- and fourth-order Legendre polynomials with $x_i = \hat{\mathbf{u}}_i.\hat{\mathbf{n}}$, where the unit vector $\hat{\mathbf{u}}_i$ denotes the orientation of particle i and the unit vector $\hat{\mathbf{n}}$ the nematic director. If the nematic director $\hat{\mathbf{n}}$ is *a priori* unknown, order parameters can be extracted from the largest positive eigenvalue of averaged dyadic vector products, known as the Saupe tensor in the case of S_2 [42,43]. However, if just the existence of a preferential direction is of interest, an orientational correlation can also be identified by using inner products of particle orientations $x_i = \hat{\mathbf{u}}_j.\hat{\mathbf{u}}_k$ instead. With the latter approach, averaging over scalar products of particle orientations $\hat{\mathbf{u}}_j$ and $\hat{\mathbf{u}}_k$ has to be limited according to periodic boundary conditions fulfilling the minimum image convention. In this work, we identify the isotropic-nematic phase transition by comparison of order parameters calculated via the latter approach.

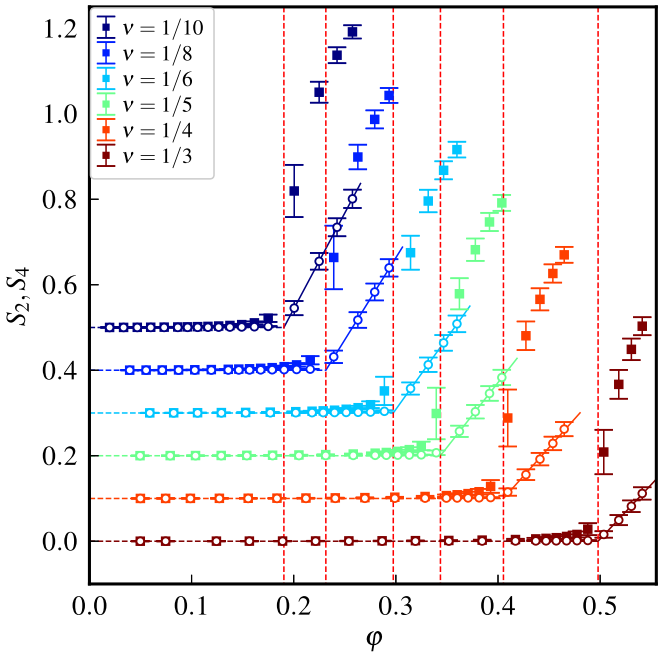

FIG. 3. Nematic order parameters S_2 (closed squares) and S_4 (open circles) in dependence on the volume fraction φ for six different aspect ratios ν separated by arbitrary offsets. The dashed red lines indicate the critical volume fractions φ_c which are roots of extrapolated, linear increasing S_4 beyond the transition to the nematic phase.

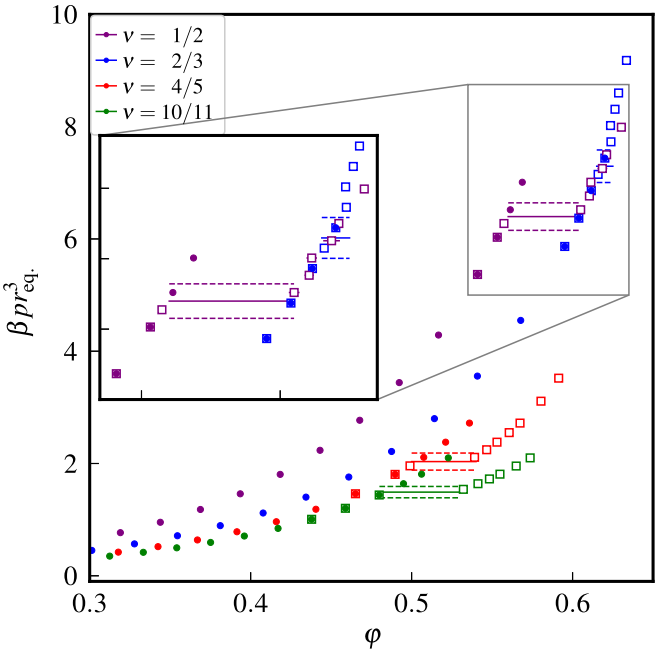

FIG. 4. Equation-of-state data for four different aspect ratios ν from compression (closed circles) and expansion (open squares) simulations. The coexistence pressures and their uncertainties are displayed as horizontal solid and dashed lines. While at aspect ratio $\nu = 1/2$ a transition from a SM2 phase to the isotropic phase is observed, for the less anisometric particles a transition from a plastic solid (PS) to the isotropic phase occurs.

Since the increase of S_4 with the volume fraction by transition to the nematic structure is much more pronounced than that of S_2, the critical volume fractions are determined by linear extrapolation of S_4 to its root. This approach is visualized in Fig. 3, where for a better display the data are separated by arbitrary offsets. The critical volume fractions φ_c as indicated by red dashed lines are compiled in Table I.

2. Isotropic-solid phase transitions

For aspect ratios $\nu \geqslant 1/2$, phase transitions from isotropic to either monoclinic SM2 phases or plastic solids (PS) occur. In contrast to the isotropic-nematic phase transition, which can be determined by compression of a disordered configuration, isotropic-solid phase transitions can only be determined by expansion of crystalline structures. Simulations of crystalline phases require deformation trials allowing nonorthogonal simulation boxes as enabled by appropriate transformation matrices **H** (Sec. II A). Due to the high sensitivity of the phase stability to the simulation box and the larger system-size dependence, data of crystalline phases exhibit larger uncertainties than those of isotropic and nematic phases. The uncertainties of coexistence pressures are estimated by pressure differences between consecutive, independent runs. The coexistence pressures at isotropic-crystalline phase transitions are displayed in Fig. 4. The respective data are compiled in Table I.

TABLE I. Phase boundaries of the isotropic phase.

ν	Phase transition	φ_c	$\beta p_c r_{\mathrm{eq}}^3$
1/10	I → N	0.190(2)	2.45(4)
1/8	I → N	0.231(2)	2.66(5)
1/6	I → N	0.297(2)	3.14(5)
1/5	I → N	0.344(2)	3.64(6)
1/4	I → N	0.405(2)	4.43(7)
1/3	I → N	0.498(2)	6.51(12)
1/2	I → SM2	0.560(5)	6.40(25)
2/3	I → PS	0.615(5)	7.30(29)
4/5	I → PS	0.500(10)	2.03(15)
10/11	I → PS	0.480(20)	1.49(10)

In contrast to Odrizola *et al.* [9], who identified the existence of a nematic phase in the limits $0.561 \leqslant \varphi \leqslant 0.565$ at aspect ratio $\nu = 1/2$ by means of replica exchange MC, we observed a direct transition from the monoclinic SM2 phase to the isotropic phase for these particles. To facilitate sufficient exchange probabilities between different replicas, the maximum size of a replica is rather limited. In contrast to Odriozala *et al.* our approach is to minimize the ensemble-size dependence using significantly larger systems instead of a higher density resolution. With exception of $\nu = 1/2$, our phase diagram reproduces that of Odriozola *et al.*

D. Equation-of-state data

Due to the absence of attractive interactions, fluidlike, hard-particle systems do not exhibit a critical point and thus are supercritical. Employing the virial series originally proposed by Kamerlingh Onnes [44] and later theoretically

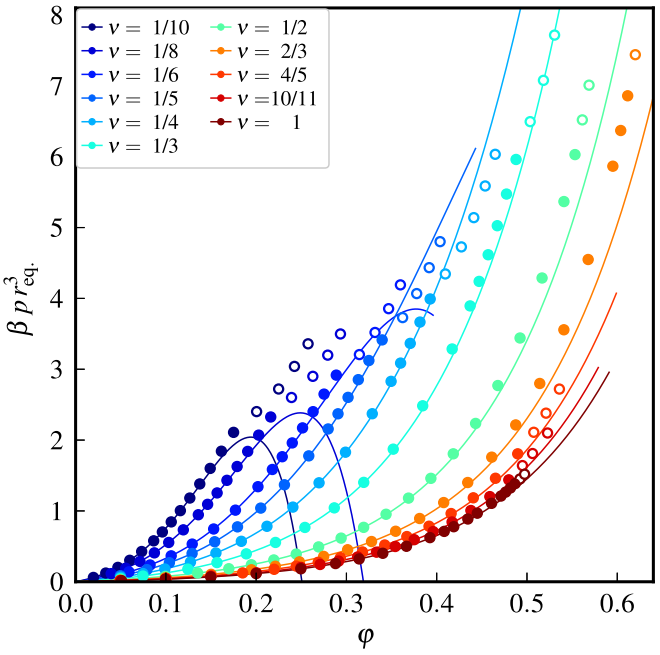

FIG. 5. Equation-of-state data for selected aspect ratios of oblate hard ellipsoids. The solid lines represent the equation of state using a virial series up to order eight. Cluster-MC data in the isotropic phase are represented by solid circles, while cluster-MC results beyond the phase boundary of the isotropic phase are displayed by open circles.

derived by Mayer [45], the real gas factor Z can be written exactly as

$$Z = \frac{p}{\varrho k_B T} = 1 + \sum_{i=2}^{\infty} B_i^* \varphi^{i-1} \tag{10}$$

if the reduced virial coefficients B_i^* are known up to infinite order i. In the virial series, the virial coefficient B_i^* of order i accounts for the contribution of i-particle interactions, i.e., clusters consisting of i particles to the real gas factor.

Depending on the particle shape, only a limited number of hard particles' virial coefficients are known. The truncation of the virial series after the highest available virial coefficient possibly leads to an inadequate description for the equation of state depending on the the volume fraction φ.

In Fig. 5, the reduced pressure $\beta p r_{\mathrm{eq.}}^3$ in dependence on the volume fraction φ resulting from cluster-MC simulations is compared to a virial approach using recently published, accurate virial coefficients up to order eight [28]. This comparison shows a severe discrepancy between simulation data and truncated virial series at high volume fractions φ. For highly anisotropic particles, the truncated virial approach even leads to unphysical, negative real gas factors.

Previously, different approaches to compensate the contributions of unknown, higher virial coefficients have been discussed. These corrections can be reevaluated quantitatively with the now available, accurate cluster-MC data.

1. Corrections for truncated virial series

Parsons [29] suggested a correction based only on the second virial coefficient of the respective geometry and the Carnahan-Starling equation of state for hard spheres [46]. As this approach leads to a simple analytical expression for the free energy, it is widely used in classical density functional theory [47]. When only few low-order virial coefficients of hard anisotropic particles were known, Nezbeda [30], Boublík [31], as well as Song and Mason [32] proposed corrections for the truncation of the virial series.

With access to the virial coefficients up to order five, Vega extended the Parsons approach by using the known virial coefficients and approximating the unknown ones by an identically rescaled Carnahan-Starling approach. Hence, a generalized Parsons approach reads as

$$Z = 1 + \sum_{i=2}^{i_{\max}} B_i^* \varphi^{i-1} + \frac{B_2^*}{B_2^{*,\,\mathrm{HS}}} \sum_{i=i_{\max}+1}^{\infty} B_i^{*,\,\mathrm{HS}} \varphi^{i-1}, \tag{11}$$

if virial coefficients up to order $i_{\max}$ are known. Hereby, essentially the Carnahan-Starling approximation for the missing virial coefficients of order $i > i_{\max}$ is rescaled by the ratio of second virial coefficients of the respective shape B_2^* and hard spheres $B_2^{*,\,\mathrm{HS}}$.

With $\varphi < 1$, for the infinite Carnahan-Starling series, the closed expression

$$\sum_{i=2}^{\infty} (i^2 + i - 2)\varphi^{i-1} = \frac{4\varphi - 2\varphi^2}{(1-\varphi)^3} \tag{12}$$

results. Herewith for any number $i_{\max}$ of known virial coefficients, a closed expression for Eq. (11) can be formulated. For $i_{\max} = 8$ this leads to

$$Z = 1 + \sum_{i=2}^{8} B_i^* \varphi^{i-1} + \frac{B_2^*}{4} \frac{2\varphi^8 (35\varphi^2 - 78\varphi + 44)}{(1-\varphi)^3}. \tag{13}$$

The comparison of Figs. 5 and 6 clearly shows that for moderately anisotropic particles with $\nu \geqslant 1/5$ the virial series with the correction according to Eq. (13) accurately describes the cluster-MC results within the phase boundaries of the isotropic phase. For intermediate aspect ratios, slight over- and underestimations at high pressures can be identified. For highly anisotropic particles with $\nu \leqslant 1/6$, however, significant deviations still occur leading as previously discussed even to unphysical, negative real gas factors. The drop of real gas factors is caused by negative virial coefficients of order $i \geqslant 5$ emerging already for moderately anisotropic particles.

Since the maximum volume fraction of the isotropic phase is comparatively small for highly anisotropic particles, higher-order virial coefficients can only contribute significantly if their moduli are extraordinarily large. As visible in Fig. 6, even rescaled higher-order virial coefficients of hard spheres cannot compensate the negative contribution of known virial coefficients: The rescaled Parsons correction based on hard spheres, adequately describing moderately anisotropic particles' equation of state, fails in the case of highly anisotropic particles.

Orientational correlations of limited range can occur in isotropic phases even if, in the thermodynamic limit, a long-range orientational correlation is absent. Whenever the orientational correlation lengths exceed the size of an i-cluster, they are not reflected in the corresponding virial

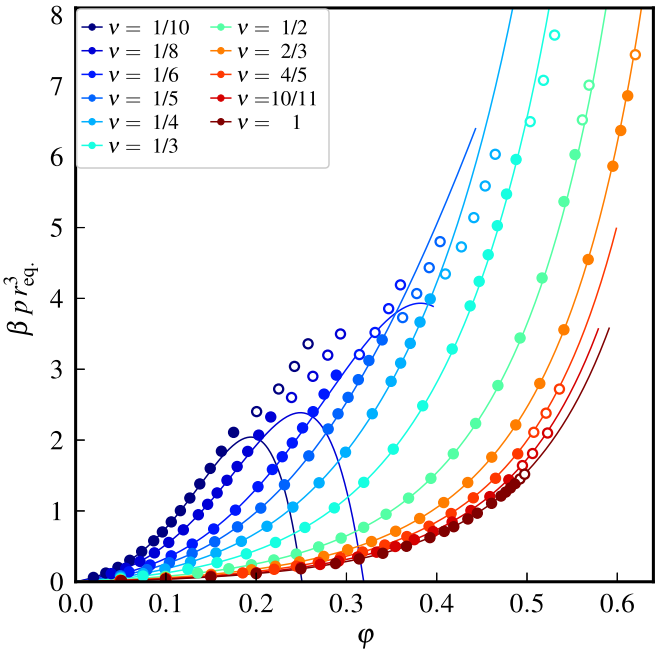

FIG. 6. Equation-of-state data for selected aspect ratios of oblate hard ellipsoids. The solid lines correspond to the virial series employing a rescaled Carnahan-Starling correction [Eq. (13)]. The equation-of-state points resulting from cluster-MC are displayed by circles, whereby closed circles are in the isotropic phase and open circles beyond the phase boundary of the isotropic phase.

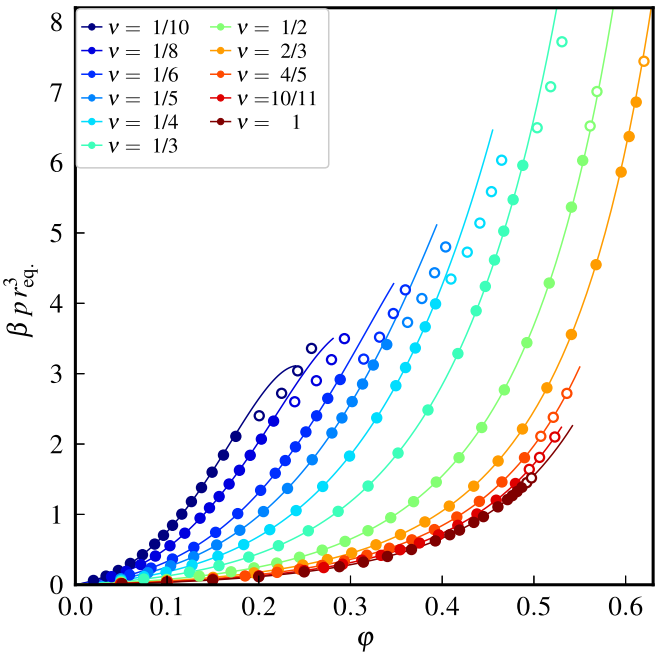

FIG. 7. Equation-of-state data for selected aspect ratios of oblate hard ellipsoids and fits using the generalized Carnahan-Starling relation [Eq. (14)]. The closed circles are equation-of-state points in the isotropic phase while open circles represent equation-of-state data beyond the phase boundary of the isotropic phase.

coefficient of order i. To adequately take the effect of orientational correlations into account, high-order up-to-now inaccessible virial coefficients are required.

Since orientational correlations do not exist for spheres and the Parsons correction only includes the second virial coefficient which is based on pair interactions, approaches based on the Parsons correction are not capable to describe the effect of increasing orientational correlation lengths emerging with progressively anisometric particles.

2. *Generalized Carnahan-Starling equation*

For hard spheres, numerous correlations for the compressibility factor using virial coefficients as well as equation-of-state data have been investigated [48]. Many of them are Padé expansions based on the Carnahan-Starling equation, where an increasing number of additional parameters improve their accordance with available data. For the exhaustively investigated hard-sphere system, Kolafa *et al.* [39] proposed a polynomial with as much as nine heuristic parameters as an accurate description of the real gas factor.

We investigate a modified Carnahan-Starling equation

$$Z = \frac{1 + \gamma_0\varphi + \gamma_1\varphi^2 - \gamma_2\varphi^3}{(1-\varphi)^3}, \tag{14}$$

where in addition to the analytically known second virial coefficient only two further parameters are needed. To approach the virial expansion in the low-density limit, the parameter γ_0 is chosen to be

$$\gamma_0 = B_2^* - 3, \tag{15}$$

which is for hard particles the excess part of the mutual excluded volume. The correlations proposed by Nezbeda [30] and Song and Mason [32] approach this low-density limit as well.

The remaining parameters γ_1 and γ_2 are obtained via least-squares fits from cluster-MC data within the boundaries of the isotropic phase (Sec. III C). The cluster-MC real gas factors and least-squares fits according to Eq. (14) are displayed in Fig. 7, and the optimum parameters γ_1 and γ_2 are compiled in Table II in dependence on the aspect ratio ν.

Despite the simplicity of this heuristical correction with only two unknown parameters, the real gas factor according

TABLE II. Parameters γ_1 and γ_2 and their uncertainties for a generalized Carnahan-Starling-type equation [Eq. (14)] for 11 different aspect ratios ν as well as density limits of the data considered.

ν	Limits	Coefficients	
		γ_1	γ_2
1/10	$0.020 < \varphi < 0.190$	61.66143(13)	333.7431(10)
1/8	$0.039 < \varphi < 0.231$	37.40249(11)	169.0247(8)
1/6	$0.059 < \varphi < 0.297$	19.00785(5)	68.07192(23)
1/5	$0.050 < \varphi < 0.344$	12.26132(8)	37.2321(3)
1/4	$0.050 < \varphi < 0.405$	7.12067(9)	17.5093(4)
1/3	$0.050 < \varphi < 0.498$	3.57926(7)	6.50072(18)
1/2	$0.050 < \varphi < 0.560$	1.593380(26)	1.88163(6)
2/3	$0.050 < \varphi < 0.615$	1.25381(12)	1.43668(24)
4/5	$0.049 < \varphi < 0.500$	1.11610(13)	1.1958(4)
10/11	$0.050 < \varphi < 0.480$	1.07955(15)	1.1336(4)
1	$0.051 < \varphi < 0.492$	1.07284(22)	1.1246(6)

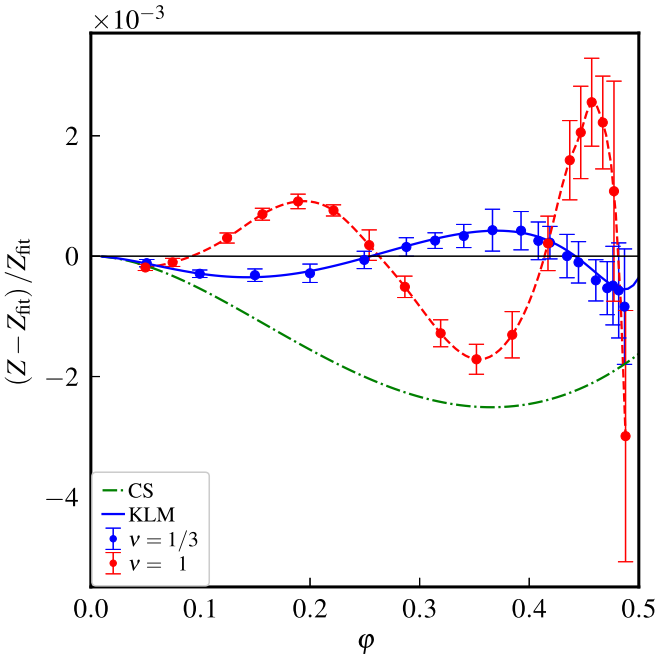

FIG. 8. Relative deviations of the modified Carnahan-Starling real gas factor Eq. (14) from simulation data exemplarily shown for aspect ratios $\nu = 1$ (hard spheres) and $\nu = 1/3$. The green line is the relative deviation from the Carnahan-Starling equation ($\gamma_1 = \gamma_2 = 1$) and the blue line the relative deviation from the Kolafa-Labík-Malijevský equation of state for hard spheres [39]. The dashed red line is a cubic spline as a guide to the eye.

to Eq. (14) is in good agreement to cluster-MC data. As expected, systematic relative deviations of less than 0.5% still exist exceeding the uncertainty of cluster-MC data as exemplarily shown in Fig. 8.

IV. SUMMARY AND OUTLOOK

In principle, equilibrium properties of hard-particle systems can be accessed via an alternative route using molecular dynamics instead [4]. Considering collisions of anisotropic particles, the equations of motion are numerically demanding. Therefore, Monte Carlo simulations requiring only the discrimination of overlap and nonoverlap configurations are a widely used approach in the case of anisotropic systems.

Despite the larger numerical effort of cluster-MC in comparison to classical MC, the significantly increased statistical accuracy as illustrated in Fig. 1 in total reduces the CPU time required to access precise data. The benefit of this technique increases with the complexity of overlap algorithms which are often the time-critical step for anisotropic shapes.

The probability of cluster formation depends in the case of hard particles on the closest surface-to-surface distance between two particles. For many geometries, a closed analytical expression for the minimum surface distance does not exist. In the case of ellipsoids, an upper and a lower limit for the minimum surface distance can be determined. Cluster formation probabilities based on both approximations lead to identical results for equation-of-state data: An approximation for this quantity is sufficient for cluster-MC simulations of ellipsoids and probably other shapes.

Using this method, the phase boundaries of the isotropic phase of oblate, hard ellipsoids of revolution are determined employing significantly larger ensembles than used before [5,9]. In addition, precise (N, p, T) equation-of-state data for the isotropic phase are obtained. This cluster-MC data are compared to the virial series considering recently published virial coefficients of oblate ellipsoids up to order eight.

For moderately anisotropic ellipsoids, the cluster-MC data excellently agree with the virial series up to moderate volume fractions (Fig. 5). The discrepancies in vicinity to the phase transition can be reduced significantly by a rescaled Carnahan-Starling correction [Eq. (13)] for the unknown virial coefficients of order $i > 8$ (Fig. 6).

For highly anisotropic particles with aspect ratio $\nu \leqslant 1/6$ even employing this correction, significant deviations from cluster-MC data are observed in the vicinity to the isotropic-nematic phase transition. At volume fractions beyond the isotropic-nematic phase transition, the virial series even predicts unphysical, negative pressures. A possible explanation are long-range orientational correlations in dense systems of highly anisotropic particles whose range is sufficiently covered only in large clusters reflected by inaccessible high orders of virial coefficients. Since orientational correlations do not exist in hard-sphere systems, any correction based on the Carnahan-Starling equation is not capable to correct these effects: Rescaling with the second virial coefficient of a highly anisotropic shape can only account for short-range orientational correlations in two-particle clusters.

Equation-of-state data of hard-particle systems are commonly described by heuristical correlations such as the Kolafa-Labík-Malijevský equation of state. For ellipsoids of revolution, different approaches have previously been published [25,30–32]. We propose a generalized Carnahan-Starling approach using the second virial coefficient and two additional parameters for each aspect ratio. Despite the simplicity of this approach, equation-of-state data are described surprisingly well within the phase boundaries of the isotropic phase.

Precise equation-of-state data resulting from cluster-MC simulations enable a quantitative analysis of truncation effects in virial approaches and commonly used corrections for the unknown, higher-order virial coefficients. Using oblate, hard ellipsoids of revolution, the capability of cluster-MC to access precise equation-of-state data of anisotropic hard particles is exemplarily demonstrated.

Systematic cluster-MC simulations of differently shaped hard particles can give insights into the importance of higher-order virial coefficients and many-particle interactions of hard particles in dependence on shape and aspect ratio for less dilute systems.

ACKNOWLEDGMENTS

P.M. gratefully acknowledges financial support by the Universität Rostock within the Ph.D. scholarship program.

[1] L. Onsager, Ann. N.Y. Acad. Sci. **51**, 627 (1949).
[2] D. Frenkel, B. M. Mulder, and J. P. McTague, Phys. Rev. Lett. **52**, 287 (1984).
[3] B. M. Mulder and D. Frenkel, Mol. Phys. **55**, 1193 (1985).
[4] A. Donev, I. Cisse, D. Sachs, E. A. Variano, F. H. Stillinger, R. Connelly, S. Torquato, and P. M. Chaikin, Science **303**, 990 (2004).
[5] C. McBride and E. Lomba, Fl. Phase Equilib. **255**, 37 (2007).
[6] P. Pfleiderer and T. Schilling, Phys. Rev. E **75**, 020402(R) (2007).
[7] M. Radu, P. Pfleiderer, and T. Schilling, J. Chem. Phys. **131**, 164513 (2009).
[8] G. Odriozola, J. Chem. Phys. **136**, 134505 (2012).
[9] G. Bautista-Carbajal, A. Moncho-Jordá, and G. Ordiozola, J. Chem. Phys. **138**, 064501 (2013).
[10] N. Metropolis, A. W. Rosenbluth, M. N. Rosenbluth, A. H. Teller, and E. Teller, J. Chem. Phys. **21**, 1087 (1953).
[11] M. N. Rosenbluth and A. W. Rosenbluth, J. Chem. Phys. **22**, 881 (1954).
[12] N. G. Almarza and E. Lomba, J. Chem. Phys. **127**, 084116 (2007).
[13] E. P. Bernard, W. Krauth, and D. B. Wilson, Phys. Rev. E **80**, 056704 (2009).
[14] M. Engel, J. A. Anderson, S. C. Glotzer, M. Isobe, E. P. Bernard, and W. Krauth, Phys. Rev. E **87**, 042134 (2013).
[15] M. Isobe and W. Krauth, J. Chem. Phys. **143**, 084509 (2015).
[16] G. Odriozola, J. Chem. Phys. **131**, 144107 (2009).
[17] N. G. Almarza, J. Chem. Phys. **130**, 184106 (2009).
[18] N. Tasios and M. Dijkstra, J. Chem. Phys. **146**, 144901 (2017).
[19] I. W. Hamley, J. Chem. Phys. **95**, 9376 (1991).
[20] J. Roller, A. Laganapan, J.-M. Meijer, M. Fuchs, and A. Zumbusch, Proc. Natl. Acad. Sci. USA **118**, e2018072118 (2021).
[21] A. Isihara, J. Chem. Phys. **18**, 1446 (1950).
[22] A. Isihara and T. Hayashida, J. Phys. Soc. Jpn. **6**, 40 (1951).
[23] H. Hadwiger, Experientia **7**, 395 (1951).
[24] E. Herold, R. Hellmann, and J. Wagner, J. Chem. Phys. **147**, 204102 (2017).
[25] C. Vega, Mol. Phys. **92**, 651 (1997).
[26] X.-M. You, A. Y. Vlasov, and A. J. Masters, J. Chem. Phys. **123**, 034510 (2005).
[27] J. K. Singh and D. A. Kofke, Phys. Rev. Lett. **92**, 220601 (2004).
[28] P. Marienhagen, R. Hellmann, and J. Wagner, Phys. Rev. E **104**, 015308 (2021).
[29] J. D. Parsons, Phys. Rev. A **19**, 1225 (1979).
[30] I. Nezbeda, Chem. Phys. Lett. **41**, 55 (1976).
[31] T. Boublík, Mol. Phys. **42**, 209 (1981).
[32] Y. Song and E. A. Mason, Phys. Rev. A **41**, 3121 (1990).
[33] M. J. Maeso and J. R. Solana, Mol. Phys. **79**, 1365 (1993).
[34] I. R. McDonald, Mol. Phys. **23**, 41 (1972).
[35] K.-K. Han and H. S. Son, J. Chem. Phys. **115**, 7793 (2001).
[36] J. W. Perram and M. S. Wertheim, J. Comput. Phys. **58**, 409 (1985).
[37] L. Paramonov and S. N. Yaliraki, J. Chem. Phys. **123**, 194111 (2005).
[38] A. Donev, F. H. Stillinger, P. M. Chaikin, and S. Torquato, Phys. Rev. Lett. **92**, 255506 (2004).
[39] J. Kolafa, S. Labík, and A. Malijevský, Phys. Chem. Chem. Phys. **6**, 2335 (2004).
[40] E. G. Noya, C. Vega, and E. de Miguel, J. Chem. Phys. **128**, 154507 (2008).
[41] See Supplemental Material at http://link.aps.org/supplemental/10.1103/PhysRevE.105.014125 for the comparison of available equation-of-state data for oblate hard ellipsoids of revolution with our cluster-MC data (Sec. S-I) and data for the reduced pressures and related real gas factors (Sec. S-II).
[42] R. Eppenga and D. Frenkel, Mol. Phys. **52**, 1303 (1984).
[43] E. Lomba, C. Martín, N. G. Almarza, and F. Lado, Phys. Rev. E **71**, 046132 (2005).
[44] H. Kamerlingh Onnes, Proc. K. Ned. Akad. Wet. **4**, 125 (1902).
[45] J. E. Mayer, J. Chem. Phys. **5**, 67 (1937).
[46] N. F. Carnahan and K. E. Starling, J. Chem. Phys. **51**, 635 (1969).
[47] J. Wu and Z. Li, Annu. Rev. Phys. Chem. **58**, 85 (2007).
[48] A. Mulero, C. Galán, and F. Cuadros, Phys. Chem. Chem. Phys. **3**, 4991 (2001).